

# Does the Redshift Distribution of *Swift* Long GRBs Trace the Star-Formation Rate?

Ali M. Hasan, Walid J. Azzam

Department of Physics, College of Science, University of Bahrain, Sakhir, Bahrain

Email: wjazzam@uob.edu.bh, wjazzam@gmail.com

**How to cite this paper:** Hasan, A.M. and Azzam, W.J. (2024) Does the Redshift Distribution of *Swift* Long GRBs Trace the Star-Formation Rate? *International Journal of Astronomy and Astrophysics*, **14**, 20-44. <https://doi.org/10.4236/ijaa.2024.141002>

**Received:** February 3, 2024

**Accepted:** March 22, 2024

**Published:** March 25, 2024

Copyright © 2024 by author(s) and Scientific Research Publishing Inc. This work is licensed under the Creative Commons Attribution International License (CC BY 4.0).

<http://creativecommons.org/licenses/by/4.0/>



Open Access

## Abstract

Gamma-ray bursts (GRBs) are extremely powerful explosions that have been traditionally classified into two categories: long bursts (LGRBs) with an observed duration  $T_{90} > 2$  s, and short bursts (SGRBs) with an observed duration  $T_{90} < 2$  s, where  $T_{90}$  is the time interval during which 90% of the fluence is detected. LGRBs are believed to emanate from the core-collapse of massive stars, while SGRBs are believed to result from the merging of two compact objects, like two neutron stars. Because LGRBs are produced by the violent death of massive stars, we expect that their redshift distribution should trace the star-formation rate (SFR). The purpose of our study is to investigate the extent to which the redshift distribution of LGRBs follows and reflects the SFR. We use a sample of 370 LGRBs taken from the *Swift* catalog, and we investigate different models for the LGRB redshift distribution. We also carry out Monte Carlo simulations to check the consistency of our results. Our results indicate that the SFR can describe the LGRB redshift distribution well for high redshift bursts, but it needs an evolution term to fit the distribution well at low redshift.

## Keywords

Gamma-Ray Bursts, Redshift Distribution, Star-Formation Rate

## 1. Introduction

Although more than 50 years have passed since the first paper on gamma-ray bursts (GRBs) was published [1], we still have many questions regarding their nature and characteristics. They are the focus of many research studies due to their potential as cosmological probes [2]-[8]. GRBs are traditionally classified into two main types: long GRBs (LGRBs) with  $T_{90} > 2$  s and short GRBs (SGRBs) with  $T_{90} < 2$  s [9], where  $T_{90}$  is the observed duration during which 90% of the

fluence is detected. It is theorized that the origin of LGRBs is the core-collapse of massive stars, while SGRBs are thought to originate from compact object mergers [10] [11] [12]. Hence, it is expected that there will be a correlation between the star formation rate (SFR) and the LGRB formation rate, which encouraged researchers to investigate the redshift distribution of GRBs, and especially that of LGRBs.

However, it is important to note that the connection between the SFR and the LGRB redshift distribution is a controversial one, with many conflicting results in the literature. The controversy lies in whether there is an observed excess of GRBs at low or high redshift compared to what is implied by the SFR. The study by [13] is one of the first major contributions to this problem. Although the connection between the SFR and LGRB redshift distribution had been studied before, see for example [14], the study by [13] is one of the first to account for completeness and to place constraints on the GRB luminosity function and its evolution. Their study found evidence for a possible luminosity or density evolution of LGRBs compared to what is expected from the SFR [13]. A recent study, but with a larger data sample, by [15] found similar results. An earlier study by [16], which utilized 127 LGRBs observed by the *Swift* satellite, found an excess in GRBs at low redshift compared to the SFR. Although some studies backed the low-redshift excess claims [17] [18] [19] [20], other studies found an excess in GRBs, not at low redshift, but at high redshift [21] [22].

Moreover, many studies have opposed the excess GRB accounts, especially at low redshifts. The study by [23] was one of the earliest to do so, where they carried out Monte Carlo simulations and compared their results with previously published claims of low redshift excess – the aforementioned [16] [19] studies. They showed that the excess GRBs result from the incompleteness of the dataset, and that a complete dataset shows no excess in GRBs. The study by [23] also conducted a non-parametric  $C^-$  investigation. However, their non-parametric study seems misleading as discussed by [24] who made an in-depth study about the non-parametric methods and how their misuse can lead to incorrect results. They analyzed datasets of previous GRB luminosity/redshift evolution studies, like the previously mentioned [16] [18] [20] [23]. They found that many studies underestimated the detection threshold of GRB satellites which resulted in incomplete datasets, and hence showed an excess in GRBs. They also created a Monte Carlo simulation, which they found to agree with the Monte Carlo simulations conducted by [23]; in other words, excess GRBs resulted from incomplete datasets. The investigation by [25] also found no excess GRBs at any redshift.

More recently, the excess GRBs at low redshift claims have started to re-emerge. They are mainly driven by studies conducted by [26] [27]. In the first study, [26] formed two sets of GRBs composed of 54 and 79 LGRBs, with 61% and 67% completeness, respectively. They found an excess of LGRBs at low redshift, even with the completeness of the dataset taken into consideration. The second study [27] focused on potential reasons for this excess of LGRBs. They

split their datasets into low and high luminosity LGRBs. They found that the high luminosity LGRB dataset follows the SFR without any excess, while the low luminosity LGRB dataset did show an excess of LGRBs at low redshifts. They argue that their results may hint at new origins for low luminosity LGRBs, thus disconnecting the LGRB formation rate from the SFR. Interestingly, there were some recent reports that suggest that LGRBs can be produced by compact object mergers, instead of massive star collapse [28] [29]. Moreover, there have been studies that investigated the effect of metallicity on the LGRB distribution and have found it to be influential [30] [31]. Perhaps these can be potential reasons for the excess GRB dilemma. Although as it stands, there is no clear answer to this problem.

The aim of our current study is to investigate the distribution of LGRBs with redshift and to fit it with several proposed models. A full LGRB data set is used without constraints, including biases in detection, to study how it is linked to the star formation rate. We aim to examine the nature of the evolution term and see how it impacts the redshift distribution of LGRBs. Section 2 provides a detailed description of our method, while Section 3 presents our results and analysis. We provide a brief conclusion in the last section.

## 2. Method

The data sample that we use is collected from the *Swift* catalog<sup>1</sup>. The data sample is composed of 370 LGRBs with  $T_{90} > 2$  s. The dataset is found in **Table A1** in Appendix A. We divided the sample into 30 bins for  $0 \leq z \leq 10$  with equal bin sizes  $dz = \frac{1}{3}$ , and we then normalized the distribution. Mathematically, the distribution of GRBs can be written as:

$$\Phi(z) = \frac{dN}{dz} = \frac{dN}{dV} \frac{dV}{dz} = A \frac{\psi_*(z)}{1+z} \phi(z) \frac{dV(z)}{dz} \quad (1)$$

where  $\psi_*(z)$  is the star-formation rate density (SFRD),  $\phi(z)$  is a term that contains all contributions to the distribution other than the SFRD,  $\frac{dV}{dz}$  is the co-moving volume element and  $A$  is a normalization constant. In this paper, we do not assign any specific “meaning” to  $\phi(z)$  and  $A$ . All possible contributions such as the luminosity function, density evolution, sensitivity of the detectors and others are included in  $\phi(z)$ . Our aim is to gain insight on the nature of  $\phi(z)$  without presuming any prior connections or contributions from other sources. This is done to focus our work on the link to the SFRD, and to evaluate how significant the other contributions are to the redshift distribution of LGRBs. We caution here that since detection bias is also considered in Equation (1), then the equation represents the GRB detection distribution, rather than the formation distribution.

The SFRD that is typically used in the literature in units of  $M_{\odot} \cdot \text{yr}^{-1} \cdot \text{Mpc}^{-3}$

<sup>1</sup>[https://swift.gsfc.nasa.gov/archive/grb\\_table/](https://swift.gsfc.nasa.gov/archive/grb_table/).

is [32] [33]:

$$\psi_*(z) = \frac{0.0157 + 0.118z}{1 + \left(\frac{z}{3.23}\right)^{4.66}} \quad (2)$$

We adopt the  $\Lambda$ CMD model in this study, which gives:

$$\frac{dV}{dz} = \frac{4\pi c D_L^2}{H_0 (1+z)^2 \sqrt{\Omega_M (1+z)^3 + \Omega_\Lambda}} \quad (3)$$

where  $D_L$  is the luminosity distance, which is given by:

$$D_L(z) = \frac{(1+z)c}{H_0} \int_0^z \frac{dz}{\sqrt{\Omega_M (1+z)^3 + \Omega_\Lambda}} \quad (4)$$

and  $H_0 = 70.8$  km/s/Mpc,  $\Omega_M = 0.27$ , and  $\Omega_\Lambda = 1 - \Omega_M = 0.73$  are the adopted cosmological parameters.

We investigated and fitted our data sample with multiple models and the goodness of the fit for each model was determined using the least  $\chi^2$  test:

$$\chi^2 = \sum_i \frac{(N_i^{\text{swift}} - N_i^{\text{cal}})^2}{\sigma_i^2} \quad (5)$$

where  $\sigma_i = \sqrt{N_i^{\text{swift}}}$  is the Poisson error (68% confidence). The best fitting model is the one that gave the least  $\chi^2$  value.

The first model that we tried was a “no contributions” model,  $\phi(z) = \text{constant}$ , with the SFRD and the cosmological model being the only contributors. Then, we tested five different contribution terms  $\phi(z)$ : a power law, a broken power law, a triple power law, an exponential term, and an exponential-power law, as follows:

$$\phi_{\text{pow}}(z) = (1+z)^\alpha \quad (6)$$

$$\phi_{\text{broken}}(z) = \begin{cases} \frac{(1+z)^\alpha}{(1+r_1)^\alpha} & \text{for } z \leq r_1 \\ \frac{(1+z)^\beta}{(1+r_1)^\beta} & \text{for } z > r_1 \end{cases} \quad (7)$$

$$\phi_{\text{triple}}(z) = \begin{cases} \frac{(1+z)^\alpha}{(1+r_1)^\alpha} & \text{for } z \leq r_1 \\ \frac{(1+z)^\beta}{(1+r_1)^\beta} & \text{for } r_1 < z \leq r_2 \\ \frac{(1+r_2)^\beta (1+z)^\gamma}{(1+r_1)^{\beta_2} (1+r_2)^\gamma} & \text{for } r_2 \leq z \end{cases} \quad (8)$$

$$\phi_{\text{exp}}(z) = e^{\mu z} \quad (9)$$

$$\phi_{\text{exp-pow}}(z) = (1+z)^\alpha e^{\mu z} \quad (10)$$

where  $\alpha, \beta, \gamma, \mu, r_1$ , and  $r_2$  are the optimization parameters<sup>2</sup>. Although we do not force any specific form on  $\phi(z)$ , the expressions that we selected and chose to investigate are based on our intuitive expectations of the insight that they might provide. The broken and triple power laws were selected to give insight on how the distribution behaves at different redshift ranges. The power and exponential laws were selected to be compared with the broken/triple power law to see if the evolution is region specific, or generic to the whole distribution.

In this work, we chose two optimization methods. The first was a fitting method. The fitting was done for  $\alpha, \beta, \gamma, \mu$ , while  $r_1$  and  $r_2$  were found by looping over them and finding the optimal values that minimize  $\chi^2$ . The second method involved using the Metropolis-Hastings Markov Chain Monte Carlo (MCMC) algorithm [34]. The method used is described by Foreman-Mackey and Hogg and utilizes their Python libraries `emcee`<sup>3</sup> and `corner.py`<sup>4</sup> [35] [36]. The log of the likelihood function that we wish to maximize is of the form:

$$\ln \mathcal{L} = -\frac{1}{2} \sum_i \left[ \frac{(N_i^{\text{swift}} - N_i^{\text{cal}})^2}{\sigma_i^2} \right] = -\frac{1}{2} \chi^2. \quad (11)$$

Then  $\chi^2$  can be calculated as follows:

$$\chi^2 = -2 \ln \mathcal{L} \quad (12)$$

Here maximizing the likelihood function is equivalent to minimizing the  $\chi^2$  value. However, since the models used include different numbers of parameters, the Akaike information criterion (AIC) was used to assess the goodness of the fits and to compare the different models [37] [38]:

$$\text{AIC} = 2k + \chi^2 = 2k - 2 \ln(\mathcal{L}) \quad (13)$$

where  $k$  is the number of parameters. The better fitting model is the one that minimizes the AIC value.

We then used the MCMC simulations to fit the data to the following:

1) A new SFRD-like function—call it the GRB detection density function (GRB-DD):

$$\psi_{\text{GRB}}(z) = \frac{\alpha + \beta z}{1 + \left(\frac{z}{\gamma}\right)^\delta} \quad (14)$$

2) A broken power law (see Equation (7)).

3) A triple power law (see Equation (8)).

4) An exponential-power law (see Equation (10)).

For each case, we report the mean of the probability distribution and its deviation, the best fitting value, the  $\chi^2$  value, and the AIC.

### 3. Results

The normalized redshift distribution of the data sample used is shown in **Figure 1(a)**.

<sup>2</sup>Note that the best fitting parameters for different cases are expected to be different.

<sup>3</sup><https://emcee.readthedocs.io/en/stable/>.

<sup>4</sup><https://corner.readthedocs.io/en/latest/>.

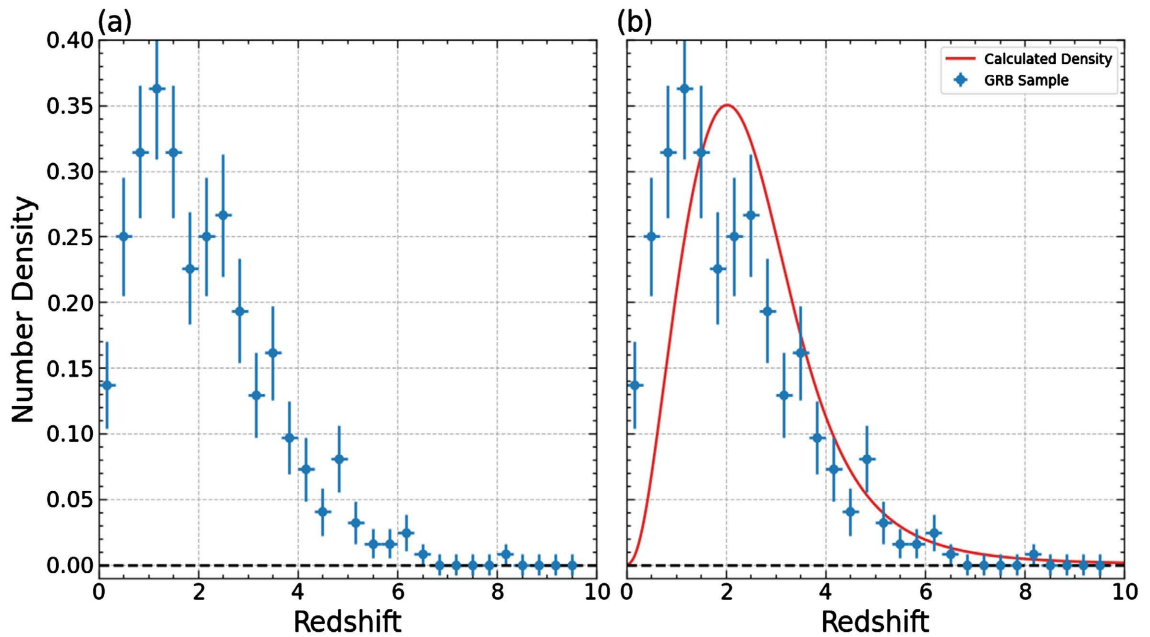


**Figure 1.** Shows (a) the redshift distribution of the GRB data set and (b) a comparison between the calculated no evolution GRB number density and the redshift distribution. Note that both the calculated density and the redshift distribution were normalized.

The main highlight of the results is the immediate spike of the number density, peaking at  $z \sim 1.25$ . Comparing that with the density calculated with no evolution (**Figure 1(b)**), we can see that the “no evolution” density peaks at  $z = 2$  with a subtle increase compared to the *Swift* data. Focusing on the low and high redshift regions, we notice the calculated density matches the *Swift* distribution at high redshifts. However, at low redshifts it is a shifted version of the *Swift* data, shifted to the right by about  $\Delta z \sim 0.5$ . To solve this issue, one might shift the density left but that would not solve the problem, as then it would underestimate the number density at  $z \gtrsim 4$ , which presents the main issue with this model. We need a term  $\phi(z)$  to be included in the density that scales it at low redshift while maintaining a good fit at high redshifts, like the SFRD (**Figure 1(b)**).

### 3.1. Fitting Results

We fitted the data sample with the proposed functions (Equations (6) to (10)), and we extracted the relevant parameters. The results are shown in **Table 1**. Based on the AIC test, the best fit occurred when we used the triple power law, the second best fit when we used the broken power law, and the third best fit when we used the exponential-power law. The power law and the exponential cases show very poor fitting. These results highlight the need for an additional  $\phi(z)$  factor and suggest that it is redshift “region” specific.

### 3.2. MCMC Results

The MCMC results are shown in **Table 2**. It is notable that the results agree mostly with the fitting results found (within  $1\sigma$ ) and lead to the same conclu-

sion. Thus, we can conclude that the results are consistent with each other. All proposed models show good fitting, with the triple power law showing the best fit. **Figure 2** plots all the models for comparison.

Now focusing on the variation between the fitting of the contributions at low and high redshifts, we notice that the results show a significant difference between the two redshift regions. This is clearly exhibited by the fitting and MCMC results, particularly in the broken power law and the triple power law cases. These cases mainly split the distribution into two regions, separated at around  $z \sim 1.75$ . Below  $z \lesssim 1.75$ , there is a high contribution from  $\phi(z)$  with powers  $\alpha = -2.56^{+0.41}_{-0.54}$  (broken power law), and  $\alpha = -5.36^{+2.60}_{-2.12}$  and  $\beta = -2.01^{+0.91}_{-0.50}$  (triple power law). Meanwhile, for  $z \gtrsim 1.75$ , the contribution from  $\phi(z)$  becomes much less impactful with values  $\beta = 0.00^{+0.30}_{-0.31}$  (broken power law) and  $\gamma = 0.06^{+0.30}_{-0.29}$  (triple power law).

We see the same behavior with the GRB-DD fit. The values for  $\beta, \gamma$ , and  $\delta$  that we found coincide with the literature reported values (see Equation (2)) within  $1\sigma$  ( $2\sigma$  in the case of  $\beta$ ). The major difference is in  $\alpha$ , with the value found by MCMC being  $\alpha = 2.88^{+1.28}_{-1.37}$  compared to the literature reported value

**Table 1.** The parameters calculated by fitting for the different cases studied with their standard deviations (if applicable).

	$\alpha$	$\beta$	$\gamma$	$\mu$	$r_1$	$r_2$	$\chi^2$	AIC
Only SFRD Contribution	-	-	-	-	-	-	83.948	---
Power Law	$-1.242 \pm 0.166$	-	-	-	-	-	50.964	52.964
Broken Power Law	$-2.845 \pm 0.276$	$0.043 \pm 0.244$	-	-	1.780	-	15.748	21.748
Triple Power Law	$-7.117 \pm 1.078$	$-2.595 \pm 0.297$	$-0.016 \pm 0.249$	-	0.500	1.800	8.184	18.184
Exponential	-	-	-	$-0.271 \pm 0.054$	-	-	66.960	68.960
Exponential-Power	$-3.742 \pm 0.466$	-	-	$0.767 \pm 0.134$	-	-	23.684	27.684

**Table 2.** The MCMC optimization results. The table includes the mean of the probability distribution and its deviation, the best fitting value, the  $\chi^2$  value, and the AIC value for each case. The corresponding contour plots of each case can be found in Appendix B.

		$\alpha$	$\beta$	$\gamma$	$\delta$	$\mu$	$r_1$	$r_2$	$\chi^2$	AIC
GRB-DD Contribution	Most Probable	$2.88^{+1.28}_{-1.37}$	$-0.20^{+0.16}_{-0.13}$	$4.74^{+0.69}_{-0.60}$	$4.94^{+1.26}_{-1.23}$	-	-	-	17.499	25.499
	Best Fit	3.190	-0.365	5.434	5.463	-	-	-		
Broken Power Law	Most Probable	$-2.56^{+0.41}_{-0.54}$	$0.00^{+0.30}_{-0.31}$	-	-	-	$1.71^{+0.23}_{-0.30}$	-	17.145	23.145
	Best Fit	-2.485	0.082	-	-	-	1.767	-		
Triple Power Law	Most Probable	$-5.36^{+2.60}_{-2.12}$	$-2.01^{+0.91}_{-0.50}$	$0.06^{+0.30}_{-0.29}$	-	-	$0.55^{+0.73}_{-0.19}$	$1.89^{+0.43}_{-0.22}$	10.657	20.657
	Best Fit	-6.280	-2.111	0.052	-	-	0.520	1.855		
Exponential-Power	Most Probable	$-3.23^{+0.48}_{-0.44}$	-	-	-	$0.67^{+0.12}_{-0.13}$	-	-	26.523	30.523
	Best Fit	-3.291	-	-	-	0.686	-	-		

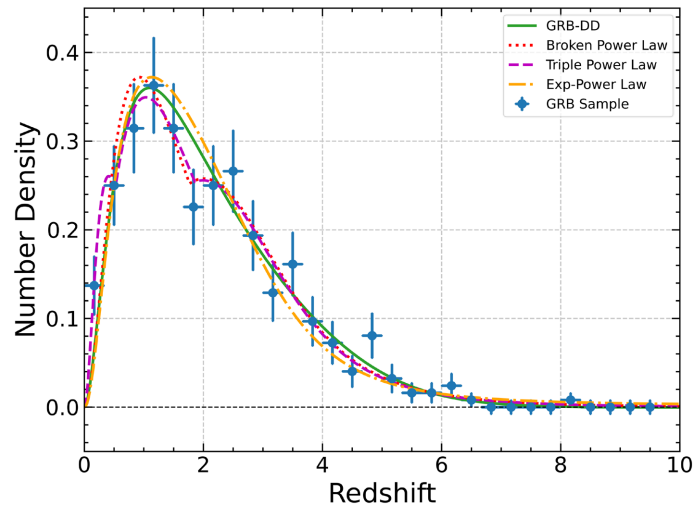


**Figure 2.** Shows number density vs redshift for all the models fit with MCMC. The best fit values were chosen for the plot of each density. It is noticeable that all the models meet at high redshifts, and their differences only occur at low redshifts.

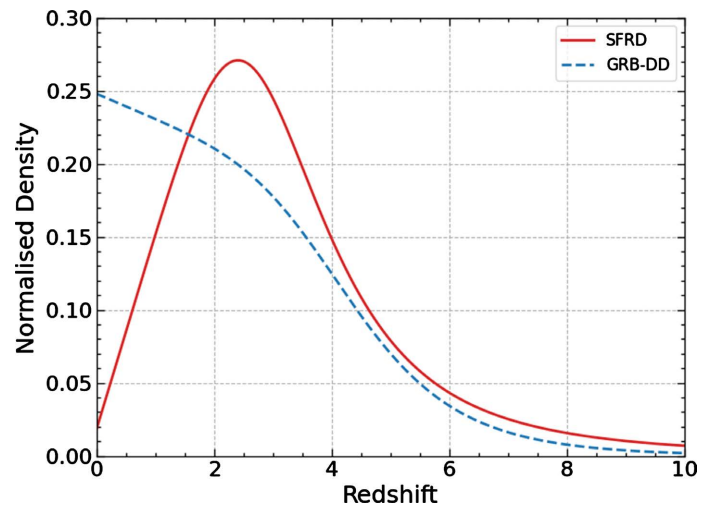


**Figure 3.** The SFRD compared to the calculated GRB-DD.

of  $\alpha = 0.0157$  (see Equation (2)). **Figure 3** shows a plot of the GRB-DD and SFRD for reference. We see that the difference between the two functions is very large at low redshifts but becomes smaller as the redshift increases to  $z > 4$ .

To summarize, our results show that the *Swift* data are consistent with the SFRD at high redshifts, and only requires an evolution term that enhances it at low redshifts. This means that if the LGRBs are to follow the SFR, then whatever factors that might affect their detection must have a stronger influence at low redshift than at high redshift. Also, it is notable that high redshift LGRBs detected by *Swift* are predominantly high luminosity ones. Hence, since our results follow the SFR at high redshifts, they support the findings of [27].

One important factor to mention that may affect the results is the classification of GRBs. In our analysis, we followed the traditional definition of LGRBs ( $T_{90} > 2$  s). This definition is widely debated among researchers with many of the

newer studies pushing for updated classifications [39]-[45]. Thus, in the future one might investigate this issue further when studying the connection between LGRBs and SFR, by considering a different classification and seeing if it would change the results found in the literature.

#### 4. Conclusion

In this paper, different models for the LGRB redshift distribution were studied. A complete data sample of *Swift* long GRBs with known redshifts was used without imposing any constraints. Our study shows that the SFRD can describe the LGRB redshift distribution for high redshift but needs an evolution term, to fit the distribution well, at low redshift. Although the data selected may have detection biases, primarily at low redshift, our results support the connection between long GRBs and stellar core-collapse. Our results indicate that the redshift distribution of the data sample fits the SFRD well at high redshifts. However, the issue of excess GRBs at low redshifts persists, because as far as our results go, they do not give us any indication about the nature of the extra contribution term  $\phi(z)$ . To verify our results, future studies should consider data sets from other satellites or a combined data sample from more than one satellite with a focus on high redshift GRBs.

#### Conflicts of Interest

The authors declare no conflicts of interest regarding the publication of this paper.

#### References

- [1] Klebesadel, R.W., Strong, I.B. and Olson, R.A. (1973) Observations of Gamma-Ray Bursts of Cosmic Origin. *The Astrophysical Journal*, **182**, L85-L88.
- [2] Dainotti, M.G., Lenart, A.L., Chraya, A., Sarracino, G., Nagataki, S., Fraija, N., Capozziello, S. and Bogdan, M. (2023) The Gamma-Ray Bursts Fundamental Plane Correlation as a Cosmological Tool. *Monthly Notices of the Royal Astronomical Society*, **518**, 2201-2240. <https://doi.org/10.1093/mnras/stac2752>
- [3] De Simone, B., Nielson, V., Rinaldi, E. and Dainotti, M.G. (2022) A New Perspective on Cosmology Through Supernovae Ia and Gamma-Ray Bursts. *Proceedings of the 16th Marcel Grossmann Meeting*, 5-10 July 2021, 3130-3140. [https://doi.org/doi:10.1142/9789811269776\\_0256](https://doi.org/doi:10.1142/9789811269776_0256)
- [4] Horvath, I., Bagoly, Z., Balazs, L.G., Hakkila, J., Horvath, Z., Joo, A.P., Pinter, S., Tóth, L.V., Veres, P. and Racz, I.I. (2024) Mapping the Universe with Gamma-Ray Bursts. *Monthly Notices of the Royal Astronomical Society*, **527**, 7191-7202. <https://doi.org/10.1093/mnras/stad3669>
- [5] Kumar, D., Rani, N., Jain, D., Mahajan, S. and Mukherjee, A. (2023). Gamma-Ray Bursts: A Viable Cosmological Probe? *Journal of Cosmology and Astroparticle Physics*, **2023**, Article No. 021. <https://doi.org/10.1088/1475-7516/2023/07/021>
- [6] Luongo, O. and Muccino, M. (2021) A Roadmap to Gamma-Ray Bursts: New Developments and Applications to Cosmology. *Galaxies*, **9**, Article No. 77. <https://doi.org/10.3390/galaxies9040077>

- [7] Schady, P. (2017) Gamma-Ray Bursts and Their Use as Cosmic Probes. *Royal Society Open Science*, **4**, Article ID: 170304. <https://doi.org/10.1098/rsos.170304>
- [8] Xu, F. and Huang, Y.-F. (2022) Probe the Universe by Using Gamma-Ray Bursts with X-Ray Plateaus. *Proceedings of the Sixteenth Marcel Grossmann Meeting*, 5-10 July 2021, 3124-3129. [https://doi.org/doi:10.1142/9789811269776\\_0255](https://doi.org/doi:10.1142/9789811269776_0255)
- [9] Kouveliotou, C., Meegan, C.A., Fishman, G.J., Bhat, N.P., Briggs, M.S., Koshut, T.M., Paciesas, W.S., Pendleton, G.N., Kouveliotou, C., Meegan, C.A., Fishman, G.J., Bhat, N.P., Briggs, M.S., Koshut, T.M., Paciesas, W.S. and Pendleton, G.N. (1993) Identification of Two Classes of Gamma-Ray Bursts. *The Astrophysical Journal Letters*, **413**, L101. <https://doi.org/10.1086/186969>
- [10] Azzam, W.J. and Al Dallal, S. (2015) Gamma-Ray Bursts: Origin, Types, and Prospects. *Journal of Magnetohydrodynamics and Plasma Research*, **20**, 367.
- [11] Dai, Z., Daigne, F. and Mészáros, P. (2017) The Theory of Gamma-Ray Bursts. *Space Science Reviews*, **212**, 409-427. <https://doi.org/10.1007/s11214-017-0423-z>
- [12] D'Avanzo, P. (2015) Short Gamma-Ray Bursts: A Review. *Journal of High Energy Astrophysics*, **7**, 73-80. <https://doi.org/10.1016/j.jheap.2015.07.002>
- [13] Salvaterra, R., Campana, S., Vergani, S.D., Covino, S., D'Avanzo, P., Fugazza, D., Ghirlanda, G., Ghisellini, G., Melandri, A., Nava, L., Sbarufatti, B., Flores, H., Piranomonte, S. and Tagliaferri, G. (2012) A Complete Sample of Bright Swift Long Gamma-Ray Bursts. I. Sample Presentation, Luminosity Function and Evolution. *The Astrophysical Journal*, **749**, Article No. 68. <https://doi.org/10.1088/0004-637X/749/1/68>
- [14] Natarajan, P., Albanna, B., Hjorth, J., Ramirez-Ruiz, E., Tanvir, N. and Wijers, R. (2005) The Redshift Distribution of Gamma-Ray Bursts Revisited. *Monthly Notices of the Royal Astronomical Society: Letters*, **364**, L8-L12. <https://doi.org/10.1111/j.1745-3933.2005.00094.x>
- [15] Lan, G.-X., Wei, J.-J., Zeng, H.-D., Li, Y. and Wu, X.-F. (2021) Revisiting the Luminosity and Redshift Distributions of Long Gamma-Ray Bursts. *Monthly Notices of the Royal Astronomical Society*, **508**, 52-68. <https://doi.org/10.1093/mnras/stab2508>
- [16] Yu, H., Wang, F.Y., Dai, Z.G. and Cheng, K.S. (2015) An Unexpectedly Low-Redshift Excess of Swift Gamma-Ray Burst Rate. *The Astrophysical Journal Supplement Series*, **218**, Article No. 13. <https://doi.org/10.1088/0067-0049/218/1/13>
- [17] Le, T. and Mehta, V. (2017) Revisiting the Redshift Distribution of Gamma-Ray Bursts in the Swift Era. *The Astrophysical Journal*, **837**, Article No. 17. <https://doi.org/10.3847/1538-4357/aa5fa7>
- [18] Lloyd-Ronning, N.M., Aykatalp, A. and Johnson, J.L. (2019) On the Cosmological Evolution of Long Gamma-Ray Burst Properties. *Monthly Notices of the Royal Astronomical Society*, **488**, 5823-5832. <https://doi.org/10.1093/mnras/stz2155>
- [19] Petrosian, V., Kitanidis, E. and Kocevski, D. (2015) Cosmological Evolution of Long Gamma-Ray Bursts and the Star Formation Rate. *The Astrophysical Journal*, **806**, Article No. 44. <https://doi.org/10.1088/0004-637X/806/1/44>
- [20] Tsvetkova, A., Frederiks, D., Golenetskii, S., Lysenko, A., Oleynik, P., Pal'shin, V., Svinkin, D., Ulanov, M., Cline, T., Hurley, K. and Aptekar, R. (2017) The Konus-Wind Catalog of Gamma-Ray Bursts with Known Redshifts. I. Bursts Detected in the Triggered Mode. *The Astrophysical Journal*, **850**, Article No. 161. <https://doi.org/10.3847/1538-4357/aa96af>
- [21] Lan, G.-X., Zeng, H.-D., Wei, J.-J. and Wu, X.-F. (2019) The Luminosity Function and Formation Rate of a Complete Sample of Long Gamma-Ray Bursts. *Monthly*

- Notices of the Royal Astronomical Society*, **488**, 4607-4613.  
<https://doi.org/10.1093/mnras/stz2011>
- [22] Perley, D.A., *et al.* (2016) The Swift Gamma-Ray Burst Host Galaxy Legacy Survey. I. Sample Selection and Redshift Distribution. *The Astrophysical Journal*, **817**, Article No. 7. <https://doi.org/10.3847/0004-637x/817/1/7>
- [23] Pescalli, A., Ghirlanda, G., Salvaterra, R., Ghisellini, G., Vergani, S.D., Nappo, F., Salafia, O.S., Melandri, A., Covino, S. and Götz, D. (2016) The Rate and Luminosity Function of Long Gamma-Ray Bursts. *Astronomy and Astrophysics*, **587**, A40.  
<https://doi.org/10.1051/0004-6361/201526760>
- [24] Bryant, C.M., Osborne, J.A. and Shahmoradi, A. (2021) How Unbiased Statistical Methods Lead to Biased Scientific Discoveries: A Case Study of the Efron-Petrosian Statistic Applied to the Luminosity-Redshift Evolution of Gamma-Ray Bursts. *Monthly Notices of the Royal Astronomical Society*, **504**, 4192-4203.  
<https://doi.org/10.1093/mnras/stab1098>
- [25] Le, T., Ratke, C. and Mehta, V. (2020) Resolving the Excess of Long GRBs at Low Redshift in the Swift Era. *Monthly Notices of the Royal Astronomical Society*, **493**, 1479-1491. <https://doi.org/10.1093/mnras/staa366>
- [26] Dong, X.F., Li, X.J., Zhang, Z.B. and Zhang, X.L. (2022) A Comparative Study of Luminosity Functions and Event Rate Densities of Long GRBs with Non-Parametric Method. *Monthly Notices of the Royal Astronomical Society*, **513**, 1078-1087.  
<https://doi.org/10.1093/mnras/stac949>
- [27] Dong, X.F., Zhang, Z.B., Li, Q.M., Huang, Y.F. and Bian, K. (2023) The Origin of Low-Redshift Event Rate Excess as Revealed by the Low-luminosity Gamma-Ray Bursts. *The Astrophysical Journal*, **958**, Article No. 37.  
<https://doi.org/10.3847/1538-4357/acf852>
- [28] Troja, E., *et al.* (2022) A Nearby Long Gamma-Ray Burst from a Merger of Compact Objects. *Nature*, **612**, 228-231. <https://doi.org/10.1038/s41586-022-05327-3>
- [29] Petrosian, V. and Dainotti, M.G. (2023) Progenitors of Low Redshift Gamma-Ray Bursts. <https://arxiv.org/abs/2305.15081>
- [30] Ghirlanda, G. and Salvaterra, R. (2022) The Cosmic History of Long Gamma-Ray Bursts. *The Astrophysical Journal*, **932**, Article No. 10.  
<https://doi.org/10.3847/1538-4357/ac6e43>
- [31] Wang, F.Y. and Dai, Z.G. (2014) Long GRBs Are Metallicity-Biased Tracers of Star Formation: Evidence from Host Galaxies and Redshift Distribution. *The Astrophysical Journal Supplement Series*, **213**, Article No. 15.  
<https://doi.org/10.1088/0067-0049/213/1/15>
- [32] Hopkins, A.M. and Beacom, J.F. (2006) On the Normalization of the Cosmic Star Formation History. *The Astrophysical Journal*, **651**, 142-154.  
<https://doi.org/10.1086/506610>
- [33] Li, L.X. (2008) Star Formation History up to  $z = 7.4$ : Implications for Gamma-Ray Bursts and Cosmic Metallicity Evolution. *Monthly Notices of the Royal Astronomical Society*, **388**, 1487-1500. <https://doi.org/10.1111/j.1365-2966.2008.13488.x>
- [34] Goodman, J. and Weare, J. (2010) Ensemble Samplers with Affine Invariance. *Communications in Applied Mathematics and Computational Science*, **5**, 65-80.  
<https://doi.org/10.2140/camcos.2010.5.65>
- [35] Foreman-Mackey, D., Hogg, D.W., Lang, D. and Goodman, J. (2013) Emcee: The MCMC Hammer. <http://dan.iel.fm/emcee>
- [36] Hogg, D.W. and Foreman-Mackey, D. (2018) Data Analysis Recipes: Using Markov

- Chain Monte Carlo. *The Astrophysical Journal Supplement Series*, **236**, Article No. 11. <https://doi.org/10.3847/1538-4365/aab76e>
- [37] Akaike, H. (1974) A New Look at the Statistical Model Identification. *IEEE Transactions on Automatic Control*, **19**, 716-723. <https://doi.org/10.1109/TAC.1974.1100705>
- [38] Liddle, A.R. (2007) Information Criteria for Astrophysical Model Selection. *Monthly Notices of the Royal Astronomical Society*, **377**, L74-L78. <https://doi.org/10.1111/j.1745-3933.2007.00306.x>
- [39] Deng, Q., Zhang, Z.-B., Li, X.-J., Chang, H.-Y., Zhang, X.-L., Zhen, H.-Y., Sun, H., Pan, Q. and Dong, X.-F. (2022) Reclassifying Swift Gamma-Ray Bursts with Diverse Duration Distributions. *The Astrophysical Journal*, **940**, Article No. 5. <https://doi.org/10.3847/1538-4357/ac9590>
- [40] Kulkarni, S. and Desai, S. (2016) Classification of Gamma-Ray Burst Durations Using Robust Model-Comparison Techniques.
- [41] Ruffini, R., Rueda, J.A., Muccino, M., Aimuratov, Y., Becerra, L.M., Bianco, C.L., Kovacevic, M., Moradi, R., Oliveira, F.G., Pisani, G.B. and Wang, Y. (2016) On the Classification of GRBs and Their Occurrence Rates. *The Astrophysical Journal*, **832**, Article No. 136. <https://doi.org/10.3847/0004-637x/832/2/136>
- [42] Salmon, L., Hanlon, L. and Martin-Carrillo, A. (2022) Two Classes of Gamma-Ray Bursts Distinguished within the First Second of Their Prompt Emission. *Galaxies*, **10**, Article No. 78. <https://doi.org/10.3390/galaxies10040078>
- [43] Steinhardt, C.L., Mann, W.J., Rusakov, V. and Jespersen, C.K. (2023) Classification of BATSE, Swift, and Fermi Gamma-Ray Bursts from Prompt Emission Alone. *The Astrophysical Journal*, **945**, Article No. 67. <https://doi.org/10.3847/1538-4357/acb999>
- [44] Tarnopolski, M. (2016) Analysis of the Observed and Intrinsic Durations of Gamma-Ray Bursts with Known Redshift. *Astrophysics and Space Science*, **361**, Article No. 125. <https://doi.org/10.1007/s10509-016-2687-2>
- [45] Zitouni, H., Guessoum, N., Azzam, W.J. and Mochkovitch, R. (2015) Statistical Study of Observed and Intrinsic Durations among BATSE and Swift/BAT GRBs. *Astrophysics and Space Science*, **357**, Article No. 7. <https://doi.org/10.1007/s10509-015-2311-x>

## Appendix A. GRB Dataset

**Table A1.** Shows the GRB dataset used.

GRB	$T_{90}$	Redshift
230506C	31.00	3.7
230414B	25.98	3.568
230116D	41.00	3.81
221226B	3.44	2.694
221110A	8.98	4.06
221009A	1068.40	0.1505
220611A	57.00	2.3608
220521A	13.55	5.6
220117A	49.81	4.961
220101A	173.36	4.61
211207A	3.73	2.272
211024B	603.5	1.1137
10822A	180.8	1.736
210731A	22.51	1.2525
210722A	50.20	1.145
210702A	138.2	1.1757
210619B	60.90	1.937
210610B	69.38	1.13
210610A	13.62	3.54
210517A	3.06	2.486
210504A	135.06	2.077
210420B	158.8	1.400
210411C	12.80	2.826
210321A	8.21	1.487
210222B	12.82	2.198
210210A	6.60	0.715
201221A	44.5	5.70
201216C	48.0	1.10
201104B	8.66	1.954
201024A	5.00	0.999
201021C	24.38	1.070
201020A	14.17	2.903
201015A	9.78	0.423

---

**Continued**

---

201014A	36.2	4.56
200829A	13.04	1.25
200205B	458.0	1.465
191221B	48.00	1.148
191019A	64.35	0.248
191011A	7.37	1.722
191004B	37.7	3.503
190829A	58.2	0.0785
190719C	185.7	2.469
190324A	28.4	1.1715
190114C	361.5	0.42
190114A	66.6	3.3765
190106A	76.8	1.86
181110A	138.4	1.505
181020A	238.0	2.938
181010A	16.4	1.39
180728A	8.68	0.117
180624A	486.4	2.855
180620B	198.8	1.1175
180510B	134.3	1.305
180404A	35.2	1.000
180329B	210.0	1.998
180325A	94.1	2.25
180314A	51.2	1.445
180205A	15.5	1.409
180115A	40.9	2.487
171222A	174.8	2.409
171205A	189.4	0.0368
171020A	41.9	1.87
170903A	29.2	0.886
170705A	217.3	2.010
170604A	26.70	1.329
170531B	164.13	2.366
170519A	216.4	0.818
170405A	164.7	3.510

---

**Continued**

---

170202A	46.2	3.645
170113A	20.66	1.968
161219B	6.94	0.1475
161129A	35.53	0.645
161117A	125.7	1.549
161108A	105.1	1.159
161017A	216.3	2.0127
161014A	18.3	2.823
160804A	144.2	0.736
160425A	304.58	0.555
160410A	8.2	1.717
160327A	28	4.99
160314A	8.73	0.726
160227A	316.5	2.38
160203A	20.2	3.52
160131A	325	0.97
160121A	12.0	1.960
151215A	17.8	2.59
151112A	19.32	4.1
151111A	76.93	3.5
151031A	5.00	1.167
151029A	8.95	1.423
151027B	80.00	4.063
151027A	129.69	0.81
151021A	110.2	2.330
150915A	164.7	1.968
150910A	112.2	1.359
150821A	172.1	0.755
150818A	123.3	0.282
150727A	88	0.313
150413A	263.6	3.2
150403A	40.90	2.06
150323A	149.6	0.593
150314A	14.79	1.758
150301B	12.44	1.5169

---

---

**Continued**

---

150206A	83.2	2.087
141225A	40.24	0.915
141221A	36.9	1.452
141220A	7.21	1.3195
141121A	549.9	1.47
141109A	200	2.993
141026A	146	3.35
141004A	3.92	0.573
140907A	79.2	1.21
140710A	3.52	0.558
140703A	67.1	3.14
140629A	42.0	2.275
140614A	720	4.233
140518A	60.5	4.707
140515A	23.4	6.32
140512A	154.8	0.725
140506A	111.1	0.889
140430A	173.6	1.60
140428A	17.42	4.7
140423A	134	3.26
140419A	94.7	3.956
140318A	8.43	1.02
140311A	71.4	4.95
140304A	15.6	5.283
140301A	31.0	1.416
140213A	60.0	1.2076
140206A	93.6	2.73
140114A	139.7	3.0
131227A	18.0	5.3
131117A	11.00	4.042
131105A	112.3	1.686
131103A	17.3	0.599
131030A	41.1	1.293
130907A	>360	1.238
130831A	32.5	0.4791

---

---

**Continued**

---

130701A	4.38	1.155
130612A	4.0	2.006
130610A	46.4	2.092
130606A	276.58	5.913
130604A	37.7	1.06
130514A	204	3.6
130511A	5.43	1.3033
130505A	88	2.27
130427B	27.0	2.78
130427A	162.83	0.34
130420A	123.5	1.297
130418A	>300	1.218
130408A	28	3.758
130215A	65.7	0.597
130131B	4.30	2.539
121211A	182	1.023
121201A	85	3.385
121128A	23.3	2.20
121027A	62.6	1.773
121024A	69	2.298
120922A	173	3.1
120907A	16.9	0.970
120815A	9.7	2.358
120811C	26.8	2.671
120805A	48.00	3.1
120802A	50	3.796
120729A	71.5	0.80
120724A	72.8	1.48
120722A	42.4	0.9586
120714B	159	0.3984
120712A	14.7	4.1745
120521C	26.7	6.0
120422A	5.35	0.28
120404A	38.7	2.876
120327A	62.9	2.81

---

**Continued**

---

120326A	69.6	1.798
120119A	253.8	1.728
120118B	23.26	2.943
111229A	25.4	1.3805
111228A	101.20	0.714
111225A	106.8	0.297
111123A	290.0	3.1516
111107A	26.6	2.893
111008A	63.46	4.9898
110818A	103	3.36
110808A	48	1.348
110801A	385	1.858
110731A	38.8	2.83
110715A	13.0	0.82
110503A	10.0	1.613
110422A	25.9	1.77
110213A	48.0	1.46
110205A	257	2.22
110128A	30.7	2.339
101225A	1088.0	0.847
101219B	34	0.5519
100906A	114.4	1.727
100902A	428.8	4.5
100901A	439	1.408
100816A	2.9	0.8034
100814A	174.5	1.44
100728B	12.1	2.106
100728A	198.5	1.567
100704A	197.5	3.6
100621A	63.6	0.542
100615A	39	1.398
100513A	84	4.772
100425A	37.0	1.755
100424A	104	2.465
100418A	7.0	0.6235

---

---

**Continued**

---

100413A	191	3.9
100316B	3.8	1.180
100302A	17.9	4.813
100219A	18.8	4.5
091208B	14.9	1.063
091127	7.1	0.490
091109A	48	3.076
091029	39.2	2.752
091024	109.8	1.092
091020	34.6	1.71
091018	4.4	0.971
090927	2.2	1.37
090926B	109.7	1.24
090812	66.7	2.452
090809	5.4	2.737
090726	67.0	2.71
090715B	266	3.00
090618	113.2	0.54
090530	48	1.266
090529	>100	2.625
090519	64	3.9
090516A	210	4.109
090424	48	0.544
090423	10.3	8.0
090418A	56	1.608
090407	310	1.4485
090313	79	3.375
090205	8.8	4.7
090113	9.1	1.7493
090102	27.0	1.547
081222	24	2.77
081221	34	2.26
081203A	294	2.1
081121	14	2.512
081118	67	2.58

---

---

**Continued**

---

081029	270	3.8479
081028A	260	3.038
081008	185.5	1.9685
081007	10.0	0.5295
080928	280	1.692
080916A	60	0.689
080913	8	6.44
080906	147	2.0
080905B	128	2.374
080810	106	3.35
080805	78	1.505
080804	34	2.2045
080721	16.2	2.602
080710	120	0.845
080707	27.1	1.23
080607	79	3.036
080605	20	1.6398
080604	82	1.416
080603B	60	2.69
080520	2.8	1.545
080516	5.8	3.2
080430	16.2	0.767
080413B	8.0	1.10
080413A	46	2.433
080411	56	1.03
080330	61	1.51
080319C	34	1.95
080319B	>50	0.937
080310	365	2.4266
080210	45	2.641
080207	340	2.0858
071122	68.7	1.14
071117	6.6	1.331
071112C	15	0.8230
071031	180	2.692

---

---

**Continued**

---

071028B	55	0.94
071021	225	2.4520
071020	4.2	2.142
071010B	>35.7	0.947
071010A	6	0.98
071003	150	1.100
070810A	11.0	2.17
070802	16.4	2.45
070714B	64	0.92
070612A	368.800	0.617
070611	12.200	2.04
070529	109.200	2.4996
070521	37.900	0.553
070508	20.900	0.82
070506	4.300	2.31
070419A	115.600	0.97
070411	121.500	2.954
070318	74.600	0.836
070306	209.500	1.497
070208	47.700	1.165
070129	460.600	2.3384
070110	88.400	2.352
070103	18.600	2.6208
061222B	40.000	3.355
061222A	71.400	2.088
061210	85.300	0.41
061121	81.300	1.314
061110B	134.000	3.44
061110A	40.700	0.758
061021	46.200	0.3463
061007	75.300	1.261
060927	22.500	5.6
060926	8.000	3.208
060912A	5.000	0.937
060908	19.300	1.8836

---

---

**Continued**

---

060906	43.500	3.685
060904B	171.500	0.703
060814	145.300	0.84
060729	115.300	0.54
060719	66.900	1.5320
060714	115.000	2.71
060707	66.200	3.43
060614	108.700	0.125
060607A	102.200	3.082
060605	79.100	3.78
060604	95.000	2.1357
060602A	75.000	0.787
060526	298.200	3.21
060522	71.100	5.11
060512	8.500	0.4428
060510B	275.200	4.9
060505	~4	0.089
060502A	28.400	1.51
060418	103.100	1.490
060223A	11.300	4.41
060218	~2100	0.0331
060210	255.000	3.91
060206	7.600	4.045
060124	~750	2.30
060123	900	1.099
060115	139.600	3.53
060108	14.300	2.03
051117B	9.000	0.481
051111	46.100	1.549
051109B	14.300	0.080
051109A	37.200	2.346
051016B	4.000	0.9364
051006	34.800	1.059
051001	189.100	2.4296
050922C	4.500	2.198

---

**Continued**

---

050915A	52.000	2.5273
050908	19.400	3.350
050904	174.200	6.10
050826	35.500	0.297
050824	22.600	0.83
050820A	26	2.612
050819	37.700	2.5043
050814	150.900	5.3
050803	87.900	0.422
050802	19.000	1.71
050730	156.500	3.96855
050724	96.000	0.257
050525A	8.800	0.606
050505	58.900	4.27
050416A	2.500	0.6535
050406	5.400	2.44
050401	33.300	2.9
050319	152.500	3.24
050318	32	1.44
050315	95.600	1.949
050223	22.500	0.5915
050126	24.800	1.29

---

## Appendix B. MCMC Contour Plots

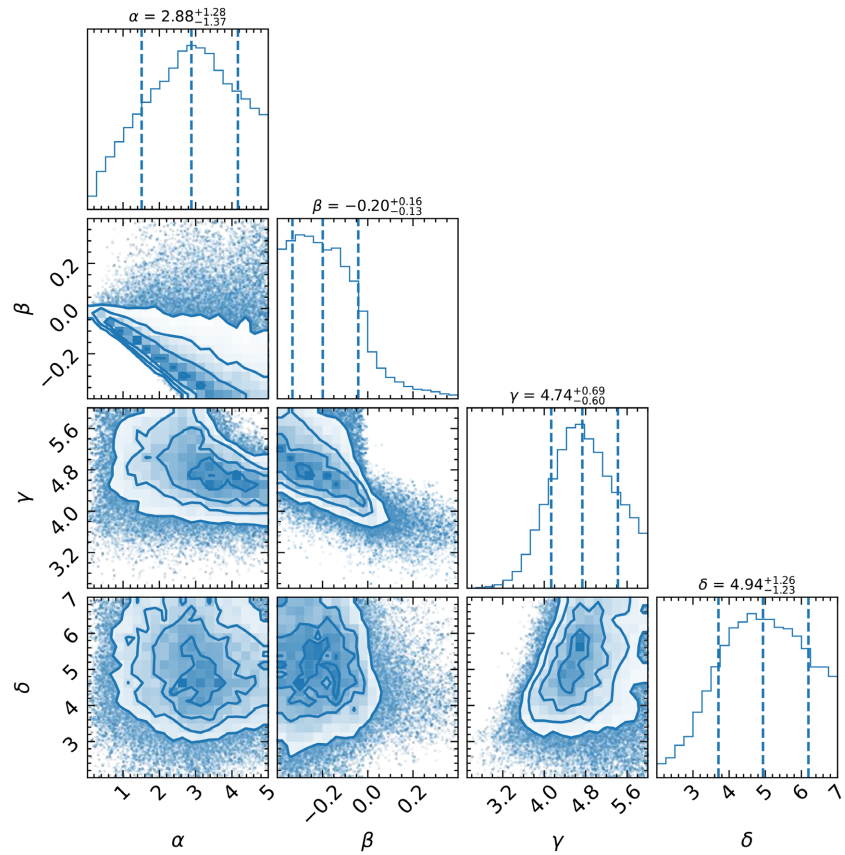


**Figure B1.** Shows the corner plot of the GRB-DD case.

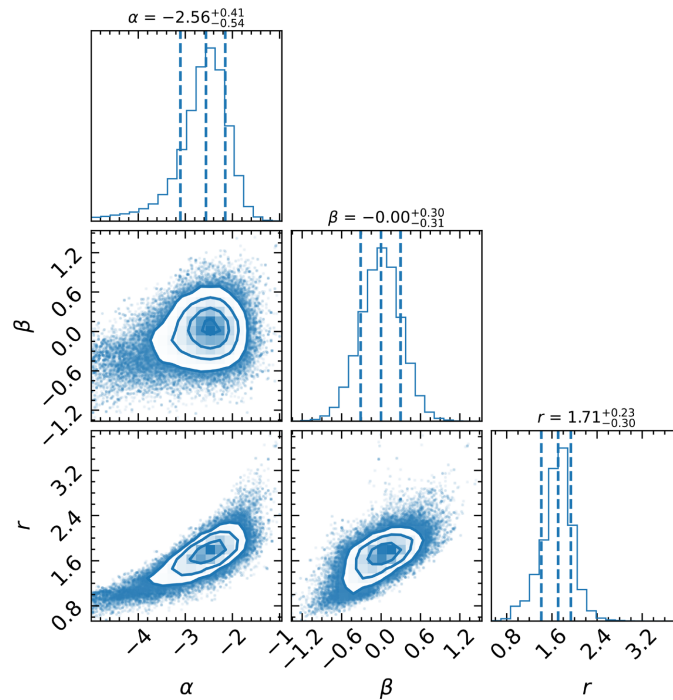


**Figure B2.** Shows the corner plot of the broken power law case.

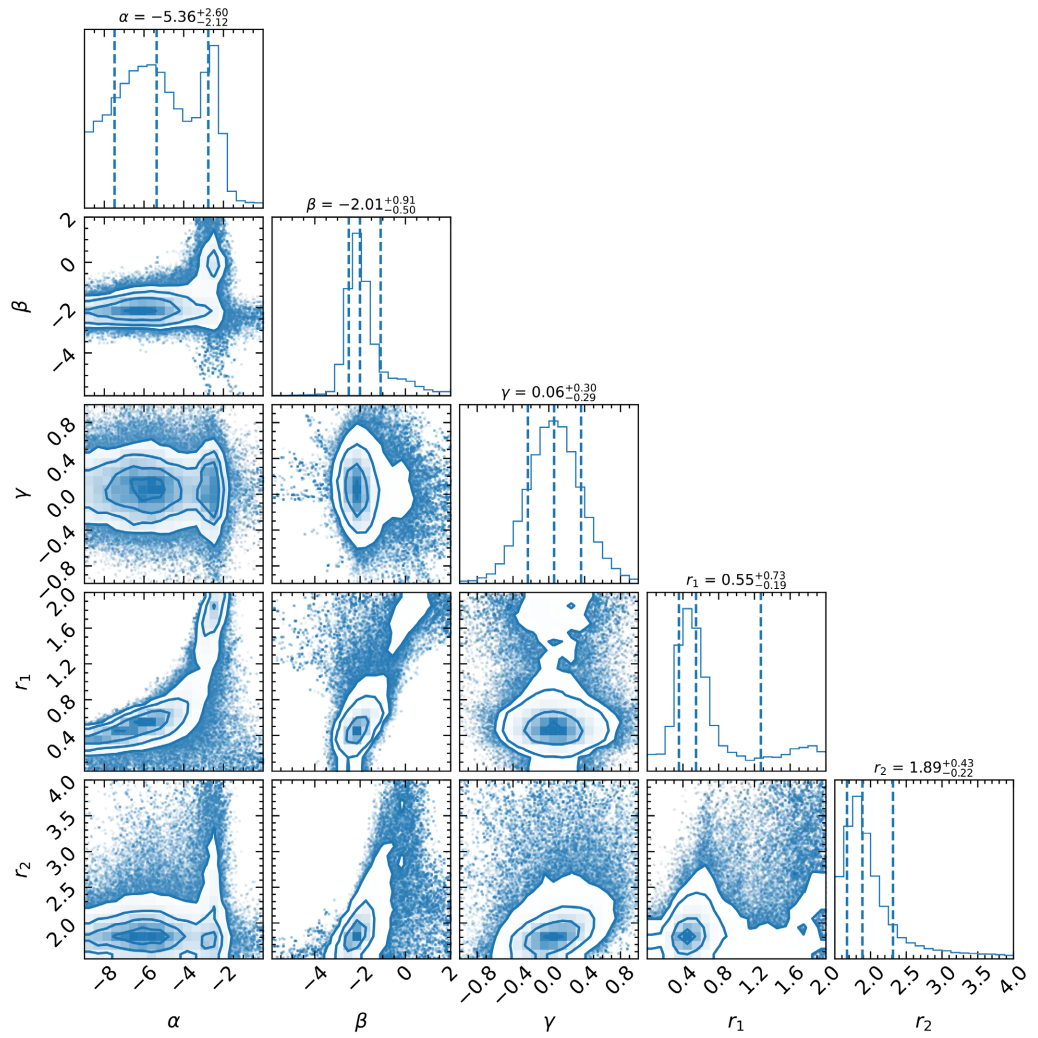


**Figure B3.** Shows the corner plot of the triple power law case.

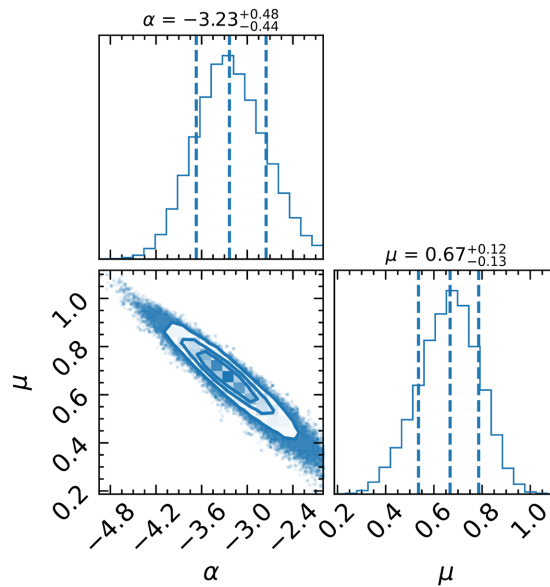


**Figure B4.** Shows the corner plot of the exponential-power law case.